3D networks of nanopores in alumina: structural and optical properties

[a] Marija Tkalčević, [a] Jordi Sancho Parramon, [a] Lovro Basioli, [a] Matej Bubaš, [b]Goran Dražić, [c]Peter Nadazdy, [c]Peter Siffalovic, [a] Maja Mičetić*

Abstract

The production of three-dimensionally ordered networks of nanopores in alumina has attracted a lot of attention due to their interesting structural properties that could be applied for a variety of applications. Here we demonstrate the production of continuous 3D networks of nanopores in alumina matrix produced by annealing of 3D networks of Ge nanowires in alumina fabricated by magnetron sputtering deposition. These nanoporous structures differ by the nanopores length, radius, and geometry of their network. The arrangement and shape of the nanopores in alumina are nearly the same as were the arrangement and shape of Ge nanowire networks, that were present in the alumina prior to the annealing. The production process is discussed and the limiting factors in the production of such nanoporous alumina films are found. We show that the unit cell parameters of the network combined with the percentage of Ge in the thin film prior to annealing, are the main limiting factors. It was found that the nanoporous structure is easily formed when the Ge atomic percentage in the film is lower than 40%, however, for the larger percentages of Ge, the alumina matrix in a unit cell is not connected to the neighboring cells in the vertical direction so the structure collapses during the annealing process. Additionally, we have shown the possibility to tune the index of refraction for alumina in a large range by varying the porosity, i.e. the parameters of the Ge nanowire network. This method allows for continuous modulation of porosity depending on the specific desired application. We believe these films could be used successfully for various sensing applications or as anti-reflective coatings for silicon-based solar cells.

Keywords: porous membrane; porous alumina; magnetron sputtering deposition; index of refraction

[a] Ruđer Boskovic Institute, 10000 Zagreb, Croatia; lovro.basioli@irb.hr (L.B.); marija.tkalcevic@irb.hr (M.T.);

[b] National Institute of Chemistry, 1001 Ljubljana, Slovenia; goran.drazic@ki.si

[c] Institute of Physics, Slovak Academy of Sciences, 845 11 Bratislava, Slovakia; peter.nadazdy@savba.sk (P.N.); peter.si alovic@savba.sk (P.S.)

1. Introduction

There has been a renewed interest in nanoporous materials because of their potential use in a variety of applications such as nanofiltration [1–4], chemical sensors [5–9], size-exclusive separation [10], water treatment [11–13], etc. Alumina (Al_2O_3)-based materials are widely investigated because alumina has excellent thermal, dielectric and mechanical properties [14] including semitransparency, insolubility, and biocompatibility [2]. Nanofiltration removes most organic molecules, nearly all viruses, most of the natural organic matter, and a range of salts. There are two major groups of nanofiltration membranes: ceramic nanofiltration membranes and polymeric nanofiltration membranes. Ceramic nanofiltration membranes are the most used inorganic membranes that have a number of advantages compared to polymeric ones. The development of ceramic membranes is mainly driven by the desire to produce membranes with higher mechanical strength, chemical and thermal tolerance, and a longer lifetime. Unlike polymeric membranes, ceramic membranes can be cleaned with aggressive chemicals, including organic solvents, or hot water steam [15].

First report of porous aluminum oxide produced by anodization of aluminum in sulphuric acid date back to the 1950s [16]. Since then electrochemical anodization was often used for the fabrication of porous alumina membranes (AAO). This method allows good control of pore size and membrane thickness with control of experimental parameters (anodization potential, electrolyte type and concentration). Brief summary of the membrane preparation using the electrochemical anodization method was given in [17]. In the work done by Zhou, Zhen Zhen, Zhen Li, and Li Li in [18] porous alumina membrane with pore diameter ranging from 30 nm to 60 nm was fabricated using two-step anodization. Elyaagoubi, Mesbah, et al. prepared AAO with a diameter in the range from 43 nm to 100 nm with a change in anodization voltage [19]. Mir, M. A., M. A. Shah, and P. A. Ganai prepared a humidity sensor based on the nanoporous anodic alumina with an average pore size of 34 nm [20]. This lack of a continuous range of available pore diameters is one of the main limitations for practical applications of AAO. Asoh, Hidetaka, Tatsuya Masuda, and Sachiko, Ono prepared α-alumina membranes over a wide range of pore diameters (from 30 nm to 350 nm) [21].

Table 1. Pore size and thickness or commonly used methods for porous alumina fabrication.

method	Pore diameter / nm	Thickness / um	Ref.
anodization	30-60	21.6 – 35.5	[18]
anodization	43-100	undefined	[19]
anodization	34	1.5 – 3.6	[20]
anodization	30-350	50	[21]
sol-gel	8-15	13.3 - 36.4	[22]
sol-gel	3.4-8.7	undefined	[23]
sol-gel	2.7-3	1.8 um - 3 um	[3]
sol-gel	1.8	4 um	[24]
sol-gel	1	undefined	[25]

Another commonly used technique for porous alumina preparation is the sol-gel method. Sol-gel (dip coating of inorganic sols) is a way of fabricating thin inorganic or polymeric coatings. Two sol-gel routes are generally described in the literature. First one is based on colloidal chemistry in aqueous media while the other utilizes the chemistry of metal-organic precursors in organic solvents [3]. Pandey, Manju, et al. prepared nanoporous alumina films on alumina substrate using sol-gel and dip-coating method [22]. The organometallic compound used for hydrolysis was aluminium sec.-butoxide. The interconnected pore structure with pore diameter in range from 8 nm to 15 nm diameter were successfully prepared by repeating the deposition several times. Chen, Xianfu, et al. prepared porous alumina membrane with an average pore diameter as small as 3 nm. Precursor used for synthesys was aluminum tri-sec-butoxide [3]. Schaep, Johan, et al. produced a mesoporous γ-Al_2O_3 membrane using

the sol-gel dipping technique that has been followed by thermal treatment with pore size in the range from 3.4 nm to 8.7 nm [23]. Akbarnezhad, Sh, Seyed Mahmoud Mousavi, and R. Sarhaddi prepared [24] fabricated alumina–titania ceramic membrane with narrow pore size distribution and average pore size of 1.8 nm and membrane thickness of 4 um. Even though a porous membrane with a pore diameter as small as 1 nm [25] can be fabricated using the sol-gel method, the thickness is usually larger than 2 um. On the other hand, porous alumina presented in this work can be made as thin as dozen nanometers.

In our previous works, we have demonstrated that annealing of regularly ordered Ge nanowire lattices can result in the formation of regularly ordered void lattices in an alumina matrix [27,28]. The annealing process induces the evaporation of Ge due to its oxidation. Therefore, the geometry of the void lattices is the same as was the Ge nanowire and quantum dot lattice before annealing. The structural properties of the pores have the same structure as Ge nanowires that were present before annealing. It was found that complete Ge desorption takes place for a critical annealing air atmosphere pressure of 10^{-3} Pa. For high vacuum annealing conditions, there is not enough oxidants present in the annealing atmosphere for the formation of a GeO_2 layer so the Ge loss process from the film is inhibited. Oxidation process of Ge QDs in alumina was investigated in [29].
Recently, we have demonstrated a method to produce self-supporting alumina nanomembranes with a 3D-ordered network of nanopores having a body-centered tetragonal ordering of its nodes and a pore diameter of about 1 nm. This method is suitable for pore size reduction to the desired value [26]. In this work, we explore the geometrical properties and applicability of these 3D networks of nanopores and the limitations in their production. We show the possibility to produce a wide range of such structures, by varying the deposition conditions of the Ge nanowire network. Control of the Ge concentration in the material prior to the annealing allows us to control the porosity of the final material, as well as the geometrical parameters of the 3D network and the nanopore radius. The main limiting factor in the production of highly-porous materials is found to be the geometry of the Ge nanowire network. For large Ge concentrations the void network becomes disconnected in the direction perpendicular to the substrate, so the structure collapse. We determine the range of the deposition parameters resulting in stable 3D networks of nanopores in alumina. In addition, we show the optical properties of these materials and the possibilities to tune the refraction index in a large range.

2. Experimental section

2.1 Sample preparation

The films were prepared by specific annealing of Ge-nanowire lattice formed in alumina matrix using magnetron sputtering deposition. Magnetron sputtering deposition is a thin film growth technique that allows precise control of over deposition parameters. The thin films contacting Ge nanowire networks were prepared by simultaneous co-deposition of Ge and Al_2O_3 using magnetron sputtering KJLC CMS-18 system. We have used Ge (99.999%) and Al_2O_3 (99.999 %) targets produced by K.J Lesker. The thin films were deposited on quartz and silicon wafers at temperatures in the range of room temperature to 600^{o}C. Before deposition substrates were degreased in an ultrasonic bath with acetone, ethanol, and isopropanol for 5 minutes to remove any dirt and grease. Before loading in the chamber substrates were cleaned with deionised water and dried in nitrogen gas after. The Ge sputtering power was tuned in the range from 2.5 to 30 W, while the power of Al_2O_3 sputtering was kept constant at 140 W, except for one case for which the power was 200 W to ensure low Ge concentration. Argon pressure was 3 Torr for all films. The deposition conditions are given in Table 2. After the deposition, the films consisted of a 3D mesh of Ge nanowires embedded in an Al_2O_3 matrix. In order to achieve Ge evaporation, samples were annealed in a low vacuum (10^{-2} mbar) environment in an electric furnace for lab heat treatment.

Table 2. Deposition parameters of the films and Ge concentrations. Sputtering power of Al_2O_3 was 140 W for all films except those indicated by * for which it was 200 W. The last row shows the measured concentrations of Ge (at. %) obtained for each sputtering power.

	P1 (2.5W)*	P2 (2.5W)	P3 (5W)	P4 (10W)	P5 (15W)	P6 (20W)	P7 (25W)	P8 (30W)
T1 (RT)	T1P1	T1P2	T1P3	T1P4	T1P5	T1P6	T1P7	T1P8
T2(200ºC)	T2P1	T2P2	T2P3	T2P4	T2P5	T2P6	T2P7	T2P8
T3(300ºC)	T3P1	T3P2	T3P3	T3P4	T3P5	T3P6	T3P7	T3P8
T4(400ºC)	T4P1	T4P2	T4P3	T4P4	T4P5	T4P6	T4P7	T4P8
T5(500ºC)	T5P1	T5P2	T5P3	T5P4	T5P5	T5P6	T5P7	T5P8
T6(600ºC)	T6P1	T6P2	T6P3	T6P4	T6P5	T6P6	T6P7	T6P8
C_{Ge} (%)	7	12	17	27	37	48	57	67

2.2 Test methods

The structural charcterization of the films was done using Transmission electron microscopy (TEM) and Grazing incidence small angle x-ray scattering (GISAXS). Optical properties of thin films were determined by Spectroscopic Ellipsometry (SE).

TEM was measured using JEOL 2010 F microscope, operated at 200 kV and equipped with a field-emission gun and a high-angle annular dark-field detector (HAADF) for Z-contrast imaging. GISAXS measurements were performed at Slovakian Academy of Sciences in Bratislava, using Bruker AXS, Nanostar setup for GISAXS. The setup is equipped with liquid-metal jet anode X-ray source (Excillum, MetalJet D2+) emitting at the wavelength of 1.34 Å. The beam collimation was performed by a parallel Montel optics (Incoatec) and two 550 µm scatterless Ge pinholes (Incoatec) 50 cm apart. The scattered X-rays were collected by a two-dimensional hybrid pixel detector (Dectris, Pilatus 300K). The samples were aligned using a positioning hexapod (Physic Instrumente) platform placed in an evacuated chamber.

Spectroscopic Ellipsometry (SE) measurements were carried out with a V-VASE ellipsometer (J.A. Woollam) in the range 0.5 - 5 eV and an angle of incidence was 70º.

3. Results and discussion

3.1 Structural analyzis

The main structural properties of the films are shown in **Fig. 1.** **Fig. 1(a)** demonstrates TEM micrograph of 3D network of Ge nanowires prior annealing and **Fig. 1(b)** shows TEM image of the same sample after annealing treatment. We can see that the structure has not changed which was confirmed with GISAXS measurements. The GISAXS maps of all investigated films as well as the photos of all samples deposited on the quartz substrate are shown in Figure 2. Practically all GISAXS maps of the films with Ge nanowires show lateral maxima, called Brag spots that confirm the formation of regular 3D networks of the nanostructures. The details of these networks containing Ge nanowires are analyzed in detail in Ref. [30]. The photo of the samples with Ge nanowires deposited on the thin quartz substrate are shown in **Fig. 2(b)**. The samples have brown colour due to the presence of Ge in them. The intensity of the colour changes with the Ge concentration, which is increasing with the Ge sputtering power (P1-P8). Three samples (T5P, T6P1 and T6P2), do not have Brag spots in GISAXS showing a lack of the formation of 3D ordered Ge network. The same samples have an almost transparent colour with some darker areas, indicating non-homogeneous deposition of

Ge, so we conclude that the deposition temperature was too high for the formation of ordered Ge nanowire network.

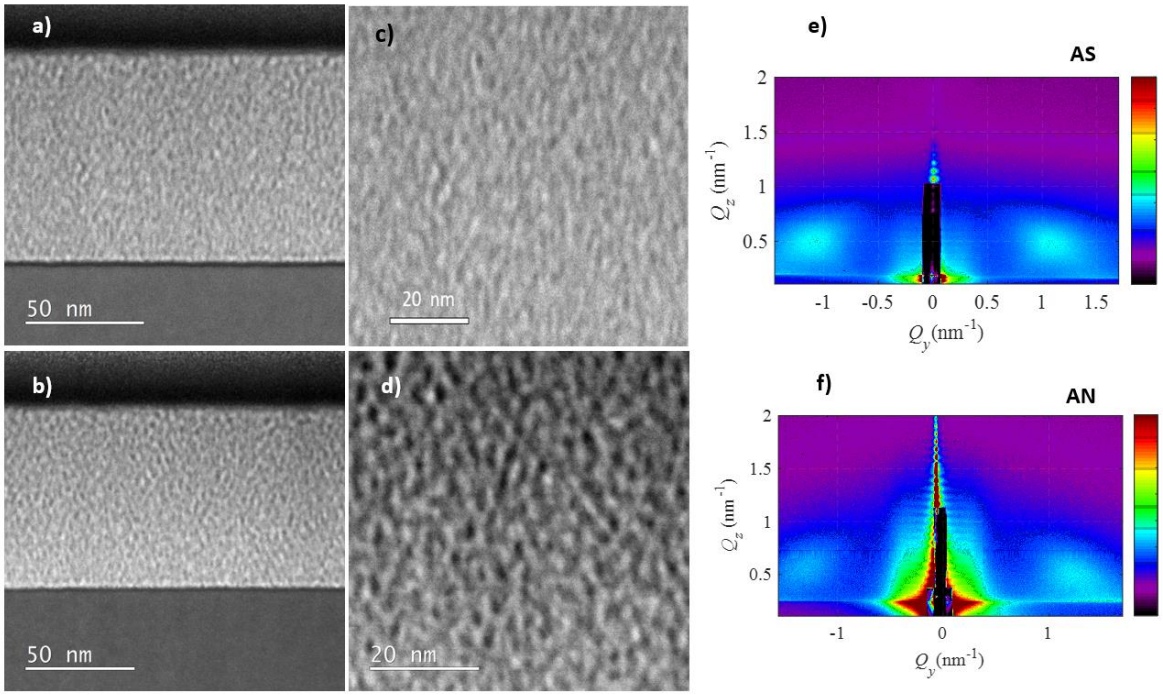

Fig. 1. HAADF TEM and GISAXS images before and after annealing. (a)-(c) TEM images before annealing; (b)-(d) TEM images after annealing; (e) GISAXS before annealing; (f) GISAXS after annealing.

The GISAXS maps and the photos of the same samples after annealing are shown in **Figure 2**(c)-(d). The GISAXS maps of the annealed films look very similar to the non-annealed ones only for the part of the samples, that are denoted by the green dashed line. Most GISAXS maps have Bragg spots at very similar positions as the non-annealed samples. The other GISAXS maps do not show Bragg spots, only the semi-circular background signal. This fact shows the destruction of the 3D network that was present before the annealing. The photos of the samples after annealing shows the change in their colour, that occurs due to the evaporation of Ge during annealing. Practically all films are fully transparent because Ge is not present in them anymore. The evaporation of Ge is confirmed also by other techniques like Time of flight elastic recoil detection analysis (TOF-ERDA) [?]. The samples deposited with the lowest Ge power are not fully transparent, showing that some Ge remained in them. This is the consequence of the formation of discontinuous Ge nanowires which disable the evaporation of Ge from them. Namely, the nanowires are the thinnest for the smallest Ge power what increases the probability of quantum dot formation instead of continuous nanowires.

We can conclude that Ge evaporated from all films where continuous Ge nanowires network was present before annealing, but the initial internal structure consisted of 3D lattices of nano-voids remained only in part of the films, that are deposited with lower Ge power (P1-P4) for all deposition temperatures, and P1-P6 for the deposition at 600^{o}C. The structure collapsed for the films deposited with the higher Ge powers, i.e. for the higher concentration of Ge present in the films before annealing (P7, P8 for all films, P5-P8 for the deposition at RT- 400^{o}C). Obviously, the increase in the deposition temperature leads to the formation of more stable structures that retain their geometry after the evaporation of Ge.

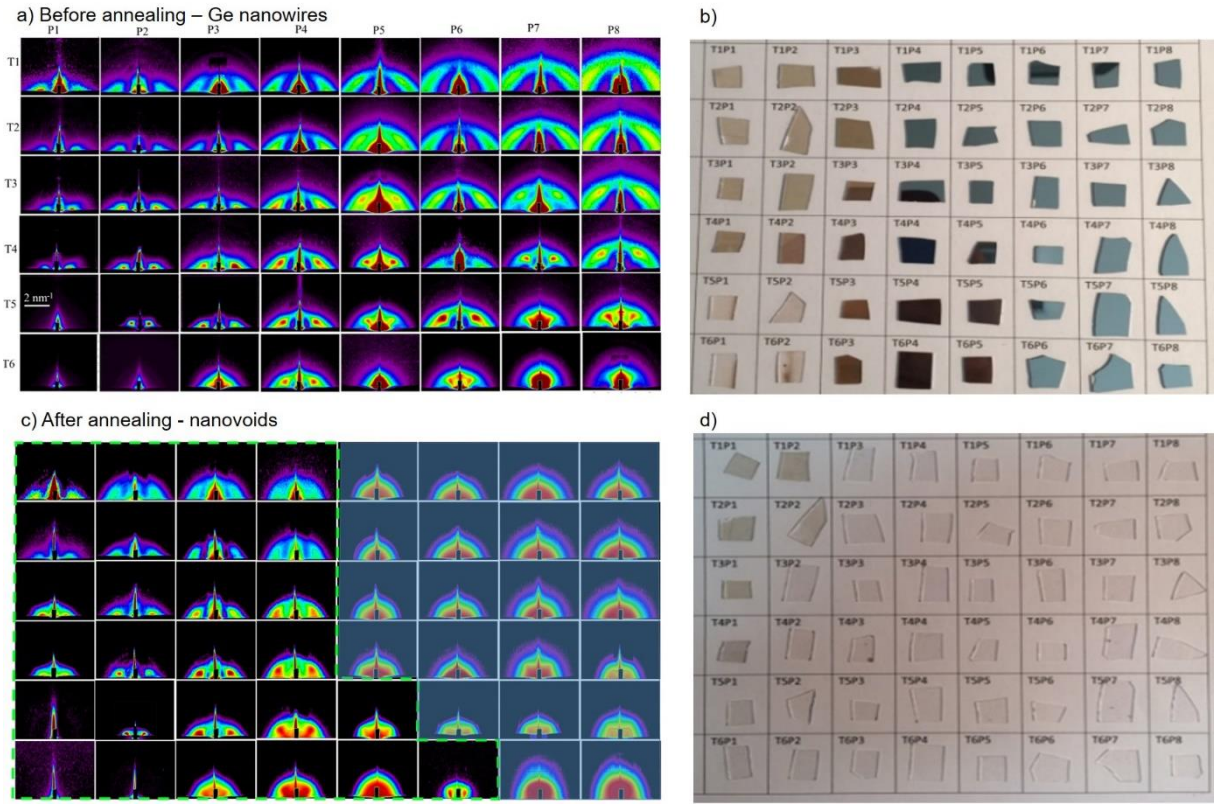

Fig. 2. Left: GISAXS maps of the (a) as-grown films containing Ge nanowires (taken from Ref. [30]); and (b) the same film after annealing at 630°C that causes desorption of Ge. Right: pictures of the films before and after annealing. After Ge leaves the samples they become fully transparent since alumina does not absorb in the visible part of spectra.

To understand the reasons for the structure collapse, we have analyzed the geometrical properties of the 3D lattices of Ge nanowires, i.e. the voids that formed after Ge evaporation. The results of the analysis are shown in **Fig. 3.** Fig. 3(a) shows the ideal structure of the film T5P2 that was stable and showed the same GISAXS maps before and after annealing. The Ge nanowires (i.e. the formed voids after annealing) are shown by red colour, while the empty space, in that case, represents the alumina matrix in which the nanostructures are embedded. When this structure is looked form the top (please see the insert of Fig. 3(a) the small hole is visible. The size of the hole is very important because the alumina matrix from two adjacent unit cells is interconnected through it. That hole actually presents the critical place for the stability of the void structure, because the hole is the place where the alumina is thinnest. The stability of the structure is actually determined by the geometrical properties of the alumina that holds the nano-voids and if the alumina is disconnected the structure collapse. The shape of the alumina inside the structure denoted by the blue box in **Fig. 3(a)** is shown by green colour. The openings in this structure indicated by blue and yellow arrows are the places where alumina is connected to the alumina from the neighboring unit cells. The openings to the unit cell in the same plane (plane parallel to the substrate) are indicated by blue arrows while the openings to the planes up and below (planes perpendicular to the substrate) are indicated by yellow arrows. These openings (i.e. their smallest part) correspond to the hole discussed above, and they are the critical points of the alumina structure).

When the Ge sputtering power is increased, the size of the hole is decreasing, which is visible form Fig. 3(b) and 3(c). Hole size is significantly reduced in **Fig. 3(b)** where the film T5P8 is shown, while it completely disappears for the film T1P8 shown in **Fig. 3(c)**. Therefore, the structure of the film T5P8 remains the same after the annealing, while the film T1P8 collapse.

The size of the critical point, i.e. the size of the hole is analysed in detail in **Fig. 4.** In **Fig. 4(a)** is shown the diameter of the hole as function deposition temperature and Ge concentration. GISAXS maps of the films showing the stable and collapsed structures are shown in **Fig. 4(b)**. The stable structures are denoted by red dashed lines in both panels. From the comparison of the determined hole sizes and the corresponding GISAXS maps, we conclude that the critical hole diameter is about 1 nm. For the smaller hole diameters, the structure collapse during annealing of Ge containing alumina.

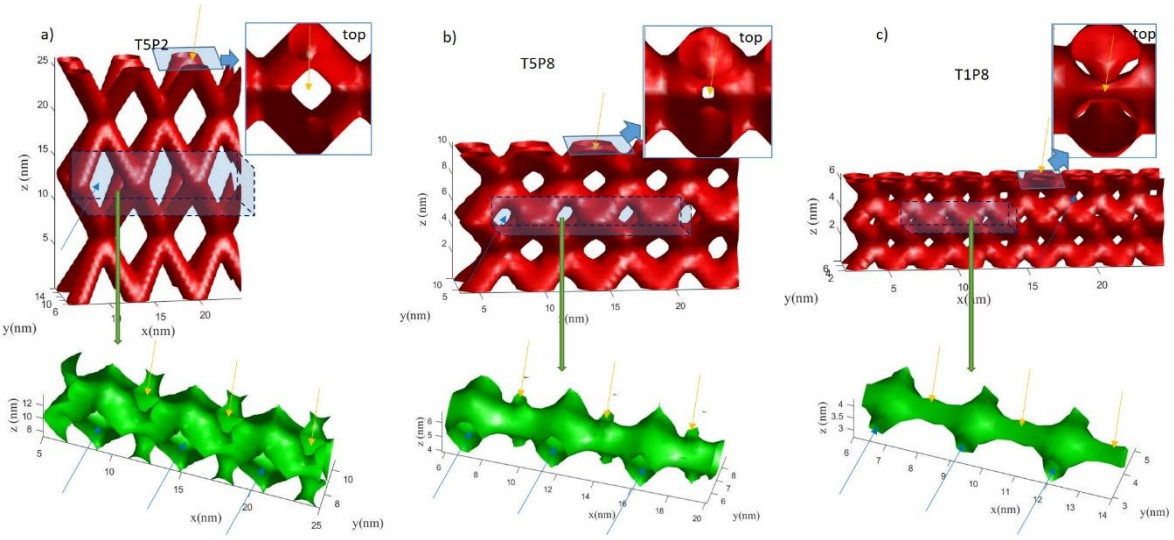

Fig. 3. Model of the structure of the nanoporous networks (the pores are shown by red colour) and the shape of the alumina matrix surrounded by the pores (shown by green colour). (a) Film T5P2; (b) T5P8; and (c) T1P8. The blue and yellow arrows indicate positions where the alumina matrix is interconnected with the alumina from the next cells in the y and z-directions respectively. The simulation shown in panel c has no opening in the z-direction, showing that the alumina matrix is not continuous for this case.

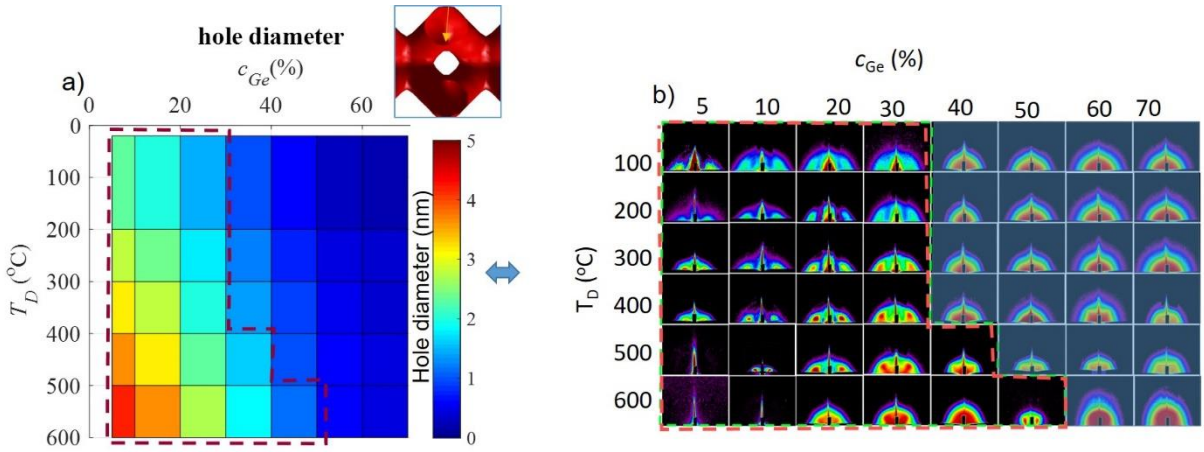

Fig. 4. (a) Dependence of the hole diameter on Ge concentration and deposition temperature; (b) GISAXS maps of samples after annealing. Samples, where porous alumina structure is preserved, are denoted with a dashed red line.

Brief summary of all results is given in **Table 3**. From these data we distinguish three cases: Ge remains in the film due to the discontinuities in the Ge nanowire network (grey fill), successful formation of Ge nanovoid lattice (green fill), and the collapse of the structure of nanovoid lattices (red fill). The volume of the formed nanovoids is very similar to the volume of Ge that was present before annealing. So, the tuning of Ge concentration enables us to simply tune the porosity of the nanowire networks. **Fig. 5.** illustrates the dependence of the material porosity on the deposition parameters.

Table 3. Structures formed after annealing of Ge nanowire network. The inset shows the legend.

	P1	P2	P3	P4	P5	P6	P7	P8
T1	T1P1	**T1P2**	**T1P3**	**T1P4**	T1P5	T1P6	T1P7	T1P8
T2	T2P1	**T2P2**	**T2P3**	**T2P4**	T2P5	T2P6	T2P7	T2P8
T3	T3P1	**T3P2**	**T3P3**	**T3P4**	T3P5	T3P6	T3P7	T3P8
T4	T4P1	**T4P2**	**T4P3**	**T4P4**	T4P5	T4P6	T4P7	T4P8
T5	T5P1	**T5P2**	**T5P3**	**T5P4**	**T5P5**	T5P6	T5P7	T5P8
T6	T6P1	T6P2	**T6P3**	**T6P4**	**T6P5**	**T6P6**	T6P7	T6P8

	3D nanopore network
	Ge remained inside the film
	3D structure destroyed
	Deposition failed

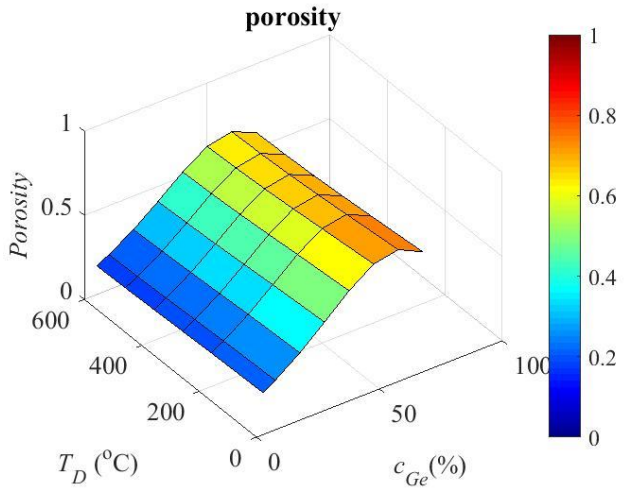

Fig. 5. Simulated porosity of the nanovoid networks vs. deposition parameters (Ge percentage c_{Ge} and deposition temperature T_D). The volume of the pores is assumed to be the same as the volume of Ge nanowires that were present before annealing.

3.2 Optical properties of porous alumina

The refraction index of the prepared nanopores networks is demonstrated in **Fig. 6. (a)-(b).** Only the films with successful formation of the nanowire network are taken into account (please see Table 2.). **Fig. 6(a)** shows the refraction index of the films differing by the initial (before annealing) Ge concentration, all of them deposited at the same temperature (600ºC). The effect of the deposition temperature for the films with similar Ge concentration on their refraction index is illustrated in **Fig. 6(b)**. The relationship between porosity and refractive index:

$$V_f = 1 - \frac{n_f^2 - 1}{n_f^2 + 2} \cdot \frac{n_s^2 + 2}{n_s^2 - 1}$$

where n_f is a refractive indexs of porous film , $n_s$is refractive indexs solid skeleton, and V_f is the volume fraction of the pores [31].

The dependence of the refraction index on the Ge concentration and deposition temperature for particular wavelengths (nm) are shown in **Fig. 6(c)** and (d) respectively. We can see that Ge concentration influences the refraction index significantly, while the temperature does not have a significant influence.

The porosity of the materials is determined from optical measurements (Spectroscopic ellipsometry) and from structural (GISAXS) data. These results are shown in **Fig. 6(e)-(f)** respectively. The data show the same trend; however small differences appear that are probably the consequence of the idealized shape of the formed nanovoids that is used in GISAXS modelling. The close relation of the porosity and Ge concentration is expected because the size of the nanovoids is determined by the size of Ge nanowires that were present before annealing.

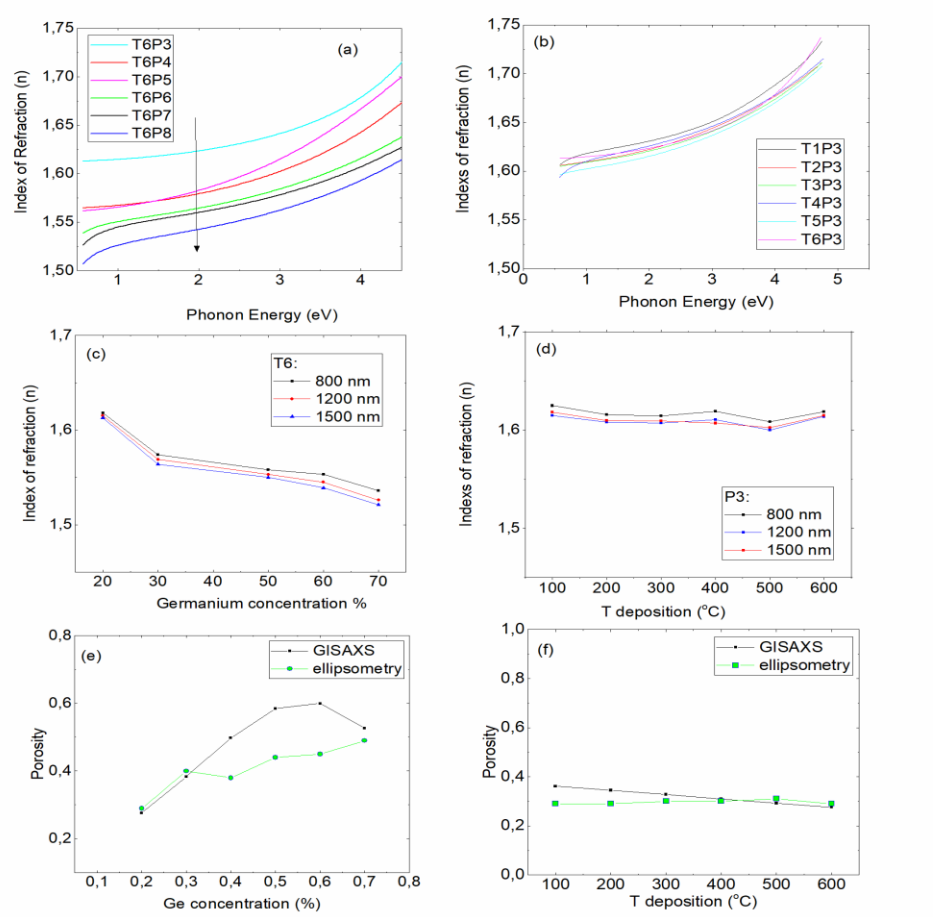

Fig 6. (a)-(b) Index of refraction as a function of phonon energy after annealing, (c)-(d) dependence of the index of refraction on deposition temperature and Ge concentration, (e)-(f) porosity calculation for series T6 and series P3 using GISAXS and Spectroscopic ellipsometry.

4. Conclusion

We have demonstrated the benefits and limitations of the production of continuous 3D networks of nanopores in the alumina matrix by annealing of 3D networks of Ge nanowires. We have shown the fabrication conditions leading to the formation of 3D ordered inter-connected meshes of nanopores with small pore sizes (about 1 nm). The limiting factor for the production of these materials is shown to be the geometry of the initially present Ge nanowire network, or more precisely the size of the interconnection channel of the alumina matrix that is present between the Ge nanowires. For smaller Ge percentages, the nonporous network easily forms, while for larger percentages, the structure collapse after Ge evaporation.

The porosity of the presented materials is simply related to the Ge concentration before the annealing process. We have demonstrated that the refractive index changes continuously as a function of the Ge concentration which allows for optical properties to be modulated depending on the specific desired application. Thin films containing Ge NWs in alumina can be fabricated on different substrates, including porous ones. We believe these films could be used successfully for various sensing applications.

[1] H.U. Osmanbeyoglu, T.B. Hur, H.K. Kim, Thin alumina nanoporous membranes for similar size biomolecule separation, J. Memb. Sci. 343 (2009) 1–6. https://doi.org/10.1016/j.memsci.2009.07.027.

[2] J. Smilek, H. Kynclová, P. Sedláček, J. Prášek, M. Klučáková, Specific permeability of nanoporous alumina membranes studied by diffusion cell technique, NANOCON 2015 - 7th Int. Conf. Nanomater. - Res. Appl. Conf. Proc. (2015) 348–353.

[3] X. Chen, W. Zhang, Y. Lin, Y. Cai, M. Qiu, Y. Fan, Preparation of high-flux γ-alumina nanofiltration membranes by using a modified sol-gel method, Microporous Mesoporous Mater. 214 (2015) 195–203. https://doi.org/10.1016/j.micromeso.2015.04.027.

[4] S. Alami-Younssi, A. Larbot, M. Persin, J. Sarrazin, L. Cot, X. Chen, W. Zhang, Y. Lin, Y. Cai, M. Qiu, Y. Fan, Gamma alumina nanofiltration membrane. Application to the rejection of metallic cations, Microporous Mesoporous Mater. 214 (1994) 195–203. https://doi.org/10.1016/0376-7388(94)00022-0.

[5] A. Yamaguchi, K. Hotta, N. Teramae, Optical waveguide sensor based on a porous anodic alumina/aluminum multilayer film, Anal. Chem. 81 (2009) 105–111. https://doi.org/10.1021/ac8015642.

[6] L. Juhász, J. Mizsei, A simple humidity sensor with thin film porous alumina and integrated heating, Procedia Eng. 5 (2010) 701–704. https://doi.org/10.1016/j.proeng.2010.09.206.

[7] A. Sciuto, M.C. Mazzillo, S. Di Franco, G. Mannino, P. Badala, L. Renna, C. Caruso, G. Korotcenkov, B.K. Cho, Z.H. Zargar, T. Islam, S. Kladsomboon, T. Kerdcharoen, P. Kuang, K. Constant, A. Yamaguchi, K. Hotta, N. Teramae, S. Shaik, A.K. Tiwari, S.A. Ramakrishna, Alcohol sensor based on gold-coated nanoporous anodic alumina membrane, Anal. Chim. Acta. 81 (2019) 105–111. https://doi.org/10.5772/60798.

[8] Z. Jin, F. Meng, J. Liu, M. Li, L. Kong, J. Liu, A novel porous anodic alumina based capacitive sensor towards trace detection of PCBs, Sensors Actuators, B Chem. 157 (2011) 641–646. https://doi.org/10.1016/j.snb.2011.05.044.

[9] C. Huang, W. Xie, M. Yang, J. Dai, B. Zhang, Optical Fiber Fabry-Perot Humidity Sensor Based on Porous Al2O3 Film, IEEE Photonics Technol. Lett. 27 (2015) 2127–2130. https://doi.org/10.1109/LPT.2015.2454271.

[10] D.L. Shimanovich, A.I. Vorobjova, D.I. Tishkevich, A. V. Trukhanov, M. V. Zdorovets, A.L. Kozlovskiy, Preparation and morphology-dependent wettability of porous alumina membranes, Beilstein J. Nanotechnol. 9 (2018) 1423–1436. https://doi.org/10.3762/bjnano.9.135.

[11] S.A. Younssi, M. Breida, B. Achiou, Alumina Membranes for Desalination and Water Treatment, in: Desalin. Water Treat., 2018. https://doi.org/10.5772/intechopen.76782.

[12] K.K.O.S. Silva, C.A. Paskocimas, F.R. Oliveira, J.H.O. Nascimento, A. Zille, Development of porous alumina membranes for treatment of textile effluent, Desalin. Water Treat. 57 (2016) 2640–2648. https://doi.org/10.1080/19443994.2015.1018333.

[13] Y. Mansourpanah, Nanofiltration membranes, 2017. https://doi.org/10.1007/978-3-642-40872-4_2207-1.

[14] S.R.C. Pinto, A.G. Rolo, M.J.M. Gomes, M. Ivanda, I. Bogdanović-Radović, J. Grenzer, A. Mücklich, D.J. Barber, S. Bernstorff, M. Buljan, Formation of void lattice after annealing of Ge quantum dot lattice in alumina matrix, Appl. Phys. Lett. 97 (2010). https://doi.org/10.1063/1.3499426.

[15] S. Benfer, U. Popp, H. Richter, C. Siewert, G. Tomandl, Development and characterization of

ceramic nanofiltration membranes, Sep. Purif. Technol. 22–23 (2001) 231–237. https://doi.org/10.1016/S1383-5866(00)00133-7.

[16] A.J. Dekker, H.M.A. Urquhart, on the Capacity of Porous Aluminum Oxide Layers, Can. J. Res. 28b (1950) 541–550. https://doi.org/10.1139/cjr50b-065.

[17] G.E.J. Poinern, N. Ali, D. Fawcett, Progress in nano-engineered anodic aluminum oxide membrane development, 2010. https://doi.org/10.3390/ma4030487.

[18] Z. Zhou, Z. Li, L. Li, Preparation and characterization of nanoporous alumina membrane made by two-step anodization, Key Eng. Mater. 396–398 (2009) 599–602. https://doi.org/10.4028/www.scientific.net/kem.396-398.599.

[19] Mesbah Elyaagoubi, Youssef Najih, Mohyeddine Khadiri, Amane. Oueriagli, Abdelkader Outzourhitb, Mustapha Mabrouki, Evolution of the Pore Size Distribution in Nanoporous Alumina Membranes with Anodization Voltage in Oxalic Acid, J. Mater. Sci. Eng. B. 5 (2015) 248–253. https://doi.org/10.17265/2161-6221/2015.5-6.007.

[20] M.A. Mir, M.A. Shah, P.A. Ganai, Nanoporous anodic alumina (NAA) prepared in different electrolytes with different pore sizes for humidity sensing, J. Solid State Electrochem. 24 (2020) 1679–1686. https://doi.org/10.1007/s10008-020-04683-2.

[21] H. Asoh, T. Masuda, S. Ono, Nanoporous -Alumina Membranes with Pore Diameters Tunable over Wide Range of 30-350 nm, ECS Trans. 69 (2015) 225–233. https://doi.org/10.1149/06902.0225ecst.

[22] M. Pandey, K. Tyagi, P. Mishra, D. Saha, K. Sengupta, S.S. Islam, Nanoporous morphology of alumina films prepared by sol-gel dip coating method on alumina substrate, J. Sol-Gel Sci. Technol. 64 (2012) 282–288. https://doi.org/10.1007/s10971-012-2855-y.

[23] J. Schaep, C. Vandecasteele, B. Peeters, J. Luyten, C. Dotremont, D. Roels, Characteristics and retention properties of a mesoporous γ-Al2O3 membrane for nanofiltration, J. Memb. Sci. 163 (1999) 229–237. https://doi.org/10.1016/S0376-7388(99)00163-5.

[24] J. Of, T. Oceanography, Sol-gel synthesis of alumina-titania ceramic membrane: Preparation and characterization, 3 (2010) 44–48.

[25] A. Larbot, S. Alami-Younssi, M. Persin, J. Sarrazin, L. Cot, Preparation of a γ-alumina nanofiltration membrane, J. Memb. Sci. 97 (1994) 167–173. https://doi.org/10.1016/0376-7388(94)00159-V.

[26] M. Tkalčević, M. Gotić, L. Basioli, M. Lihter, G. Dražić, S. Bernstorff, T. Vuletić, M. Mičetić, Deposition of thin alumina films containing 3D ordered network of nanopores on porous substrates, Materials (Basel). 13 (2020) 1–11. https://doi.org/10.3390/ma13132883.

[27] S.R.C. Pinto, A.G. Rolo, M.J.M. Gomes, M. Ivanda, I. Bogdanović-Radović, J. Grenzer, A. Mücklich, D.J. Barber, S. Bernstorff, M. Buljan, Formation of void lattice after annealing of Ge quantum dot lattice in alumina matrix, Appl. Phys. Lett. 97 (2010) 95–98. https://doi.org/10.1063/1.3499426.

[28] S.R.C. Pinto, M. Buljan, L. Marques, J. Martín-Sánchez, O. Conde, A. Chahboun, A.R. Ramos, N.P. Barradas, E. Alves, S. Bernstorff, J. Grenzer, A. Mücklich, M.M.D. Ramos, M.J.M. Gomes, Influence of annealing conditions on the formation of regular lattices of voids and Ge quantum dots in an amorphous alumina matrix, Nanotechnology. 23 (2012). https://doi.org/10.1088/0957-4484/23/40/405605.

[29] M. Tkalčević, L. Basioli, K. Salamon, I. Šarić, J. Sancho-Parramon, M. Bubaš, I. Bogdanović-Radović, S. Bernstorff, Z. Fogarassy, K. Balázsi, M. Petravić, M. Mičetić, Ge quantum dot lattices in alumina prepared by nitrogen assisted deposition: structure and photoelectric conversion efficiency, Sol. Energy Mater Sol. Cells. Uner revie (2020).

[30] L. Basioli, M. Tkalčević, I. Bogdanović-Radović, D. Goran, K. Salamon, M. Mičetić, 3D networks of Ge quantum wires in dielectric matrices, Nanomaterials. (2020).

[31] A. Vincent, S. Babu, E. Brinley, A. Karakoti, S. Deshpande, S. Seal, Role of catalyst on refractive index tunability of porous silica antireflective coatings by sol-gel technique, J. Phys. Chem. C. 111 (2007) 8291–8298. https://doi.org/10.1021/jp0700736.